ⒶAIAA

A01-31354

AIAA-2001-2732

Probe Measurements and Laser Absorption Spectroscopy on the IRS IPG3 Plasma Plume

M. Auweter-Kurtz[1], G. Herdrich[2], K. Komurasaki[3], T. Laux[4]

[1], [2] and [4]:   Institut für Raumfahrtsysteme (IRS)
Universität Stuttgart
Pfaffenwaldring 31
70550 Stuttgart
Federal Republic of Germany

[3]:   Department of Aeronautics and Astronautics
University of Tokyo,
Hongo 7-3-1, Bunkyo, Tokyo 113-0033, Japan

35th AIAA Thermophysics Conference
11-14 June 2001 / Anaheim, CA

Probe Measurements and Laser Absorption Spectroscopy on the IRS IPG3 Plasma Plume

M. Auweter-Kurtz[1], G. Herdrich[2], K. Komurasaki[3], T. Laux[4]

[1], [2] and [4]: Institut für Raumfahrtsysteme (IRS), Universität Stuttgart
Pfaffenwaldring 31, D-70550 Stuttgart
Federal Republic of Germany

[3]: Department of Aeronautics and Astronautics, University of Tokyo,
Hongo 7-3-1, Bunkyo, Tokyo 113-0033,
Japan

Abstract

The production of high enthalpy flows in a stationary manner requires plasma wind tunnels using plasma generators. Magnetoplasmadynamic generators (MPG), thermal arcjet devices (TPG) and inductively heated plasma generators (IPG) have been developed at IRS for different atmospheres, different atmospheric regimes and/or different basic investigations.

The absence of electrodes enables the use of IPGs for basic TPS material tests (e.g. catalycity) and the simulation of re-active atmospheres such as of Mars or Venus atmosphere.

With IPG3 an rf-source is provided where the coil is closer to the plasma than it was with previous designs. Therefore, the electromagnetic field loss is reduced. The water cooling system surrounds both the induction coil and the plasma container. This paper describes the design of IPG3 and the experimental results using O_2. test cases with pure O_2 plasma were investigated using the absorption spectroscopy system of the Department of Aeronautics and Astronautics, University of Tokyo, in combination with a Pitot pressure probe and a material sample support system of IRS, Universität Stuttgart. Number density and translational temperature distributions of atomic oxygen were obtained from the measured absorption line profiles including the triplet absorption lines of atomic oxygen OI at 777.19, 777.41, 777.54 nm. The test at an ambient pressure of 500 Pa include Pitot probe measurements and a temperature measurement using a sintered silicon carbide (SSiC) material sample. Additionally, probe measurements were performed at a low pressure condition (50Pa). Here, no suitable laser absorption measurements could be made as the plasma jet's diameter became too large.

---

[1]Professor, Senior Member AIAA, IRS, interim head of the institute
[2]Research engineer, IRS, PhD student
[3]Associate Professor, Department of Aeronautics and Astronautics
[4]Research engineer, IRS, PhD student

1. Introduction

A variety of stringent requirements upon technology are imposed by both space travel to a rather close Earth orbit and to more distant celestial bodies such as the planets of our solar system. Among those requirements there are the high temperature effects occuring during atmospheric entries. Here, spacecrafts encounter gases at velocities of even more than ten km/s, thereby being subjected to great heat loads. This makes it necessary to use high temperature thermal protection systems (TPS) to prevent the destruction of the space vehicle. Both TPS and environment (plasma) during the entry have to be investigated by means of computational and ground facility based simulations. Such ground facilities are the five IRS plasma wind tunnels PWK 1-5 that reproduce the thermal, aerodynamic and chemical load on the surface of a space vehicle entering a celestial body's atmosphere. MPGs enable gas flows at high enthalpy levels. They are mainly used to investigate the erosion of radiation-cooled heat shield materials like C-C or C-SiC as well as the behavior of ablative materials under thermal and chemical loads. Two IRS plasma wind tunnels are operated with MPGs. Furthermore, a TPG producing moderate enthalpies and higher stagnation pressures to simulate the follow-on flight path is in use [1, 2].

As an IPG uses non-contact heating by induction currents, exceptionally pure plasma flows of any gases can be produced. Therefore, the application of an IPG delivers two major advantages. First, researchers are aware that the catalytic behavior of TPS materials is one of the main topics to be investigated in the future. A main part of the heat flux seen by a TPS material derives from the recombination of atomic plasma species. Using the IPG, the related heat flux measurements are not falsified by impurities as with the electrode plasma generators. Furthermore, the catalytic mechanisms of single gases such as of O_2 and N_2 [3, 4] in the case of air in an atmosphere can be investigated. Fig. 1 shows a typical pure oxygen plasma plume of IPG3 at 500 Pa ambient pressure, an oxygen mass flow rate of 3 g/s and at an anode voltage U_A=6250 V. The resonant circuit was adjusted to nominal 650 kHz

1

using a 5-turn coil with 7 capacitors each of 6 nF (see description below).
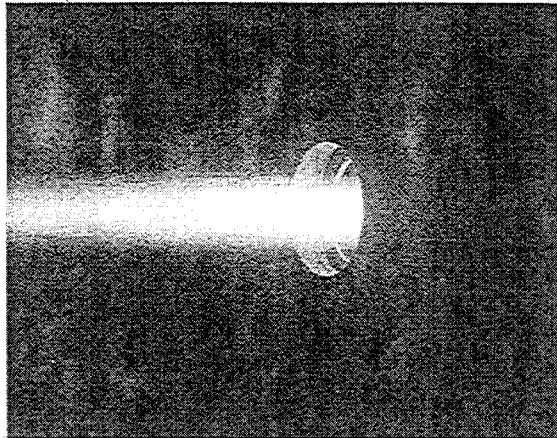
Fig. 1: IPG3 Oxygen plasma plume at ambient pressure of 500 Pa (anode power 106 kW)

In addition, applications in the range of plasma diagnostics on ground and in situ (flight experiments) such as heat flux measurements using materials with different, but well known catalycities can be performed. Here, it is possible to determine the atomic species concentrations within the plasma [5, 6]. For the direct investigation of the plasma wind tunnel plume's composition, a quantitative and non-intrusive measurement is feasible. Such powerful non-intrusive measurement techniques and methods like emission spectroscopy, laser-induced fluorescence (LIF) and Fabry-Perot interferometry (FPI) are used at IRS to investigate the plasma flows [7]. They are used to determine atomic and molecular density and the velocity distribution in the boundary layer. During Prof. Komurasaki's stay at IRS, the diode-laser absorption spectroscopy (D-LAS) technique [8] of the Department of Aeronautics and Astronautics was used for IRS-PWK3. This portable system is a very suitable measurement technique for the measurement of number densities and translational temperatures e.g. of O_2 [9]. The D-LAS is able to access absorbing atoms and molecules even in high temperature and/or high Mach number flows [8].

The second advantage of IPGs is to be seen in the possibility of performing atmosphere simulations for celestial bodies like Mars or Venus, where there are rather reactive gas components such as CO_2. Here, IRS has already performed high enthalpy CO_2 tests that showed that PWK3-IPG3 is able to perform re-entry simulations for atmospheres containing CO_2 [3]. A inductively heated plasma generator IPG4 equipped with a nozzle was developed and tested. This device enables the operation with CO_2 at higher total pressures while rather low mass flow rates are required. Additionally, a procedure to deactivate the explosive CO_2-plasma using N_2 as deactivator [10] was developed. This enables participation in

campaigns such as "Venus sample return missions", "Mars Mini-Probes" or "Mars Sample Return Mission" that are presently under investigation by CNES and NASA [11, 12, 13].

Powerful measurement techniques like intrusive probes and non-intrusive methods like emission spectroscopy, LIF and FPI are used to investigate the plasma flows. Besides the so-called non-intrusive measurement techniques, the mass spectrometry, electrostatic and radiation probes also belong to the group of intrusive measurement techniques. As the name already suggests, this diagnostic method is based on a suitably constructed probe being mounted in the plasma stream to be investigated. The mechanical probes are among the most important instruments for plasma-diagnostic measurements and are therefore often used. Besides the standard sample support system which carries the TPS material sample to be tested, Pitot pressure probes, aerodynamic wedge probes (Mach number determination), heat flux probes, enthalpy probes and solid-state electrolyte probes for determining the oxygen particle pressure are used to characterize the plasma. All of these probes can be installed at IRS on moveable platforms inside the plasma wind tunnels. Electrostatic probes are used to ascertain the plasma potential, electron density and temperature, energy distribution of the electrons, ion temperature, flow velocity and direction. The measurement principle is based on an active influence on the plasma boundary layer which forms on the probe. The use of radiometric probes is unavoidable when the radiation heat flux can not be neglected compared to the convective part. This is the case when during sample return missions the entry speed into the Earth's atmosphere is especially high or when the atmosphere of another celestial body to be entered contains strong radiating species, as for example the atmosphere of Titan. A general overview for the IRS plasma diagnostic tools is given in [7].

2. Set-up of PWK3 and the IPG
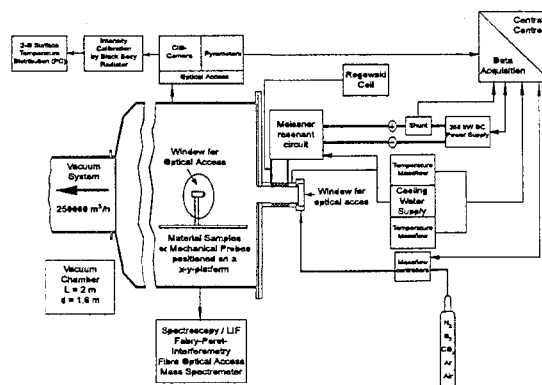
Fig. 2: Scheme of plasma wind tunnel PWK 3

The general facility set-up shown in Fig. 2 consists of the IPG plasma source and the vacuum chamber. It is about 2 m in length and 1.6 m in diameter. Optical accesses to the vacuum chamber enable the measurement of the plasma. A heat exchanger between the test chamber and the vacuum system cools down the hot plasma to protect the vacuum system from being damaged. The flat lid of PWK3 (right side of chamber, see Fig. 2) carries the IPG and the external resonant circuit, that consists of the capacitors with the connection to the plasma generator. The right side flange of the vacuum chamber is connected to the IRS vacuum pump system. It is used to simulate pressures at altitudes up to 90 km. The system consists of four stages: the first two stages are roots blowers, the third stage is a multiple slide valve type pump, and the last stage (pumping up to atmospheric pressure) is a rotary vane type pump. Total suction power of the pumps amounts to 6.000 m^3/h at atmospheric pressure and reaches about 250.000 m^3/h at 10 Pa measured at the intake pipe of the system that has a diameter of 1 m. The base pressure of the system is 0.5 Pa. The desired tank pressure can be adjusted between the best achievable vacuum and 100 kPa by removing one or more pumps from the circuit and/or mixing additional air into the system close to the pumps.

The external resonant circuit is cooled by a water-cooling circuit. With this the capacitors, which have a capacity of 6000 pF ± 20% each, and the inductor are cooled. The resonant circuit is built in Meissner type switching [14] using a metal-ceramic triode with an oscillator efficiency of about 75% [15] (see Fig. 3).
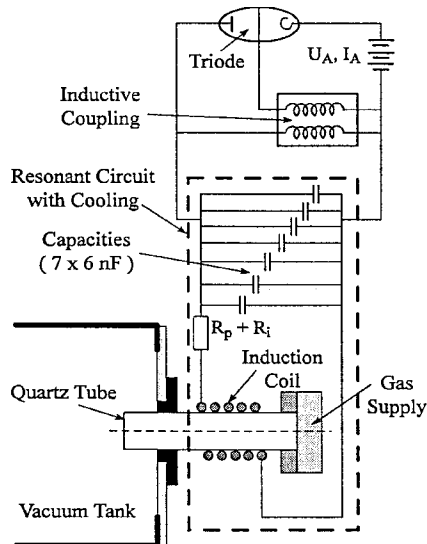
Fig. 3: Scheme of the PWK3 Meissner type resonant circuit

Its nominal frequency can be changed by switching the order or number of capacitors (see Fig. 3) as well as by the use of coils with different inductivities. The

error bars in Fig. 4, which shows the 7 different nominal frequencies using a L$_{inductor}$≈ 2 μH-coil, take into account the tolerances of the capacitors [14].
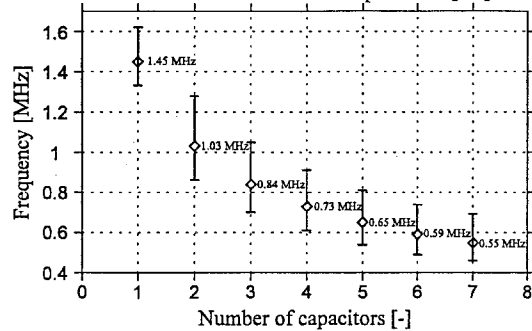
Fig. 4: Nominal operating frequencies for different capacitor switchings, L$_{inductor}$=2 μH (see text)

For the present investigations the frequency has been tuned to the nominal frequencies of 0.73 MHz (4 capacitors) using a water-cooled 5-turn coil with a length of about 120 mm. This coil geometry leads to an inductivity of about 2 μH. The whole circuit is switched to a 375 kW power supply. The incoming anode power can be adjusted by the control of the anode voltage.

Inductively heated plasma generators basically consist of an induction coil surrounding a plasma container (tube) and capacities, as schematically shown in Fig. 3. This resonant circuit is fed by an energy supply. The alternating current in the coil induces a mostly azimuthal electric field inside the tube. This electric field initiates an electric discharge in the gas that is injected at one side into the tube (see Fig. 5). The produced plasma is expanded into the vacuum chamber. The electric discharge in the plasma is carried by mostly azimuthal eddy currents. The current amplitude - and thus the Ohmic heating - strongly depends on the electric conductivity of the plasma and the resonant frequency.
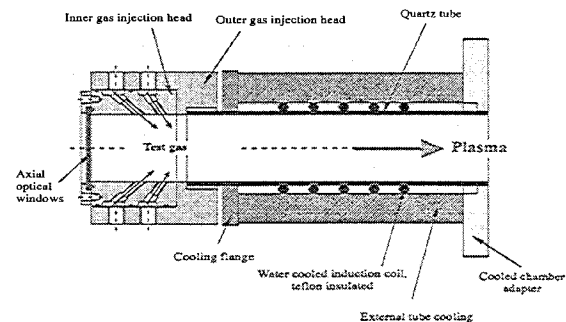
Fig. 5: View of the plasma source IPG3

The principal parts of the plasma generator IPG3 are described here. An axial optical access through the inner injection head enables investigations of the plasma inside the generator (see Fig. 5). The tube cooling system is transparent; therefore, the position of the "plasma flame" within the tube can be observed

with regard to different operating parameters such as chamber pressure, gas, mass flow and anode power. Additionally, this feature is supported by the axial optical window. The total length of IPG3 is about 0.35 m, its diameter about 0.1 m.

The quartz tube contains the produced plasma which leaves the generator through the water-cooled chamber adapter. The induction coil is connected to the external resonant circuit (Figs. 2, 3) delivering power and cooling water for IPG3. Furthermore, both the tube and the coil are surrounded by the external tube cooling, which protects the tube from overheating. The water and an additional cage around the generator serve as an rf-radiation protection shield.

3. Measurement Techniques

A variety of probes and optical diagnostic techniques that have been developed and qualified at IRS has been surveyed in the introduction of this paper. More precise descriptions have been made in [7]. The D-LAS measurement technique developed at the Department of Aeronautics and Astronautics, University of Tokyo, is a modularly built system enabling a quite simple installation. Additionally, its sub-systems are rather small such that a transport of the system from Japan to Germany was feasible. A precise description of the system is given in [9]. In the section below, the measurement techniques that have been used for the measurements presented in this paper are described.

Operational Parameter of PWK3-IPG3

The Meissner type resonant circuit is supplied by the DC anode power P_A measured during the operation of the device [2, 3, 10, 16]. The anode voltage U_A is controlled. Hence, the anode current I_A results from the load of the resonant circuit (plasma) and the accompanying operating conditions (see Fig. 3). Thermal powers such as tube cooling power and resonant circuit power are measured using resistance thermometers (see Fig. 2). They are electrically sealed and installed at an acceptable distance from the plasma source in order to prevent disturbing signals from the rf-field. Additionally, the cooling water flow rates are measured. A cavity calorimeter was developed to measure the thermal plasma power [2]. However, this exceeded the time schedule of the performed measurement campaign. It is intended to perform such a measurement in a later campaign.

Mass flow of the test gas (see Fig. 2) and the pressure of the inner gas injection head are measured as well. A modified Pearson current monitor can be used to determine the operational frequencies [17].

Probe measurements

Both the Pitot probe measurement used for this investigation and the material support system, which was used for material tests, are contained in a double-probe (see Fig. 6). It belongs to the IRS probe set developed within the Hermes program and the Collaborative Research Center 259. The geometries i.e. the outer diameter of 50 mm and the corresponding material sample diameter of 26.5 mm became the so-called European standard geometry.
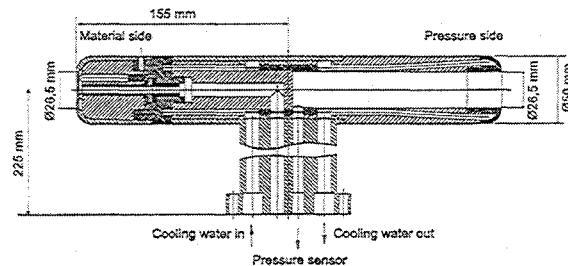
Fig. 6: Double Probe: Material support system and Pitot probe (European standard geometry)

D-LAS

The system's laser source is a tunable diode laser with an external cavity (Velocity Model 6300, New Focus, Inc.). It guarantees minimum mode hopping during the oscillation - frequency modulation. The line-width of the laser is as small as about 1 GHz. An optical isolator is used to prevent the reflected laser beam from returning into the external cavity. A Fabry-Perot etalon with an optical frequency spacing of 1.875 GHz is used to provide reference frequency spacing during the oscillation-frequency modulation. The laser beam was introduced into a test chamber through an optical fiber. A photograph of the optical system is shown in Fig. 7 (taken from [9]). After the system was transported to IRS, it performed extremely well during the on-going measurement campaign. With this and the small sizes of the system's modular components the D-LAS can be considered a transportable laser absorption system.
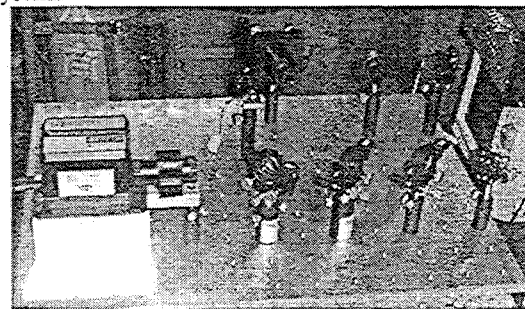
Fig. 7: Photograph of the D-LAS [9]

Figure 8 shows the set-up of the D-LAS together with PWK3. The laser incoupling was performed through the right side optical flange of PWK3. The laser collimator was fixed onto the optical window using a movable platform with a step motor in between. This enabled the measurement of radial absorption profiles.

4
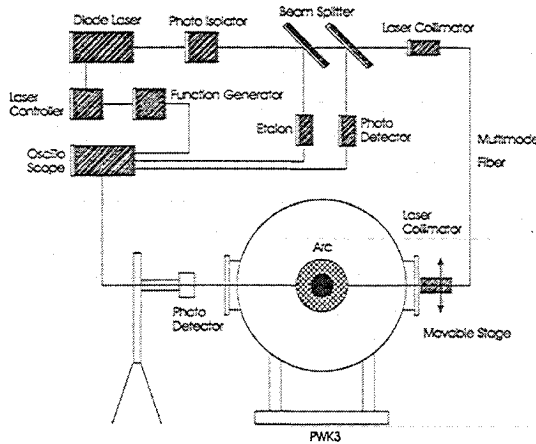
Fig. 8 Schematic set-up of the D-LAS system

The detector was put on the left side flange. Unfortunately, the minimal detectable distance from the generators outlet (see Fig. 2) was 393 mm due to the position of the right side window.

4. Measurement Theory of the D-LAS

A description of the theory of laser absorption spectroscopy has already been given in [9]. However, a brief summary is given below to simplify the reader's understanding.

Absorption coefficient

The absorption lines at 777.19, 777.41 and 777.54 nm of atomic oxygen were investigated within the tests. By measuring the absorption profile, the population density at the absorbing electronic state, which is metastable in this case, is deduced. The relationship between laser intensity I_ν and absorption coefficient k_ν is expressed by the Beer-Lambert Law as [18]

$$\frac{dI_\nu}{dx} = -k_\nu I_\nu + \varepsilon_\nu \qquad (1)$$

Here, ε_ν is emission coefficient and ν is oscillation frequency of the light. Limiting the solid angle of view very small, spontaneous emission can be eliminated. Assuming axisymmetric distributions of absorption properties in a flow, the projection of absorption coefficient along the straight line at offset y is a function of the laser absorption fraction $i_\nu(y) = \Delta I_\nu(y)/I_{\nu 0}$ as

$$\int_{-\infty}^{+\infty} k_\nu(x,y)dx = 2\int_y^R \frac{k_\nu(r)rdr}{\sqrt{r^2-y^2}} = -\ln(1-i_\nu(y)) \quad (2)$$

Using Abel-Inversion the absorption coefficient distribution is obtained as

$$k_\nu(r) = \frac{1}{\pi}\int_r^R \left(\frac{d\ln(1-i_\nu)}{dy}\right)\frac{dy}{\sqrt{y^2-r^2}} \qquad (3)$$

The local absorption coefficient is a sum of an absorption coefficient and a stimulated emission coefficient and the relationship between integrated absorption coefficient $K(r)$ and population density at the absorbing state n_i is given as [19, 20]

$$K(r) = \int k_\nu d\nu = \frac{\lambda^2}{8\pi}\frac{g_j}{g_i}A_{ji}n_i\left[1-\exp\left(-\frac{\Delta E_{ij}}{kT_{ex}}\right)\right] (4)$$

Here, i, j are lower and upper energy levels, A_{ij} is the Einstein's transition probability, g_i and g_j are statistical weights, E, k and T_{ex} are energy level, Boltzmann constant and electronic excitation temperature, respectively. The transition data of atomic oxygen at the considered wave lengths are shown in Table 1.

Table 1 Transition data of atomic oxygen

i	j	λ(nm)	E_i(cm^{-1})	E_j(cm^{-1})	g_i	g_j	A_{ji}(10^{8}s^{-1})
3s5S	3p5P	777.19	73768.20	86631.45	5	7	0.369
3s5S	3p5P	777.41	73768.20	86627.78	5	5	0.369
3s5S	3p5P	777.54	73768.20	86625.76	5	3	0.369

At 777.19 nm, for example, $\Delta E_{ij}/k$ is 18,500 K. If $T_{ex} < \Delta E_{ij}/k$, stimulated emission is neglected and Eq. (4) is simplified as

$$K = \frac{\lambda^2}{8\pi}\frac{g_j}{g_i}A_{ji}n_i \qquad (5).$$

Line profile

Generally, absorption line-shape is assumed as Voigt profile that includes Doppler broadening and pressure broadening. However, if the temperature is 5,000 K and pressure is 500 Pa, the pressure broadening is estimated three orders of magnitude smaller than the Doppler broadening. Therefore, pressure broadening is neglected [9].

The Stark broadening caused by random electric field of the electrons in plasma monotonically increases with the electron density. Then it is only noticeable in the case of high electron density plasma. In our experimental conditions, the Stark broadening of the considered lines is estimated to be less than 10MHz, which is also three orders of magnitude smaller than Doppler broadening [21].

Under these assumptions the translational temperature T_{tr} can be directly deduced from the Doppler broadening of the absorption lines [7, 9].

$$\frac{\Delta\nu_{FWHM}}{2\sqrt{\ln 2}} = \frac{\nu}{c}\sqrt{\frac{2kT_{tr}}{M_A}} \qquad (6)$$

Here, $\Delta\nu_{FWHM}$ is the full width at half maximum of the line profile, c is speed of light and M_A is atomic mass of absorbing particles.

5

In local thermal equilibrium, the ground-level number density n_0 is estimated as

$$n_0 = n_i \frac{g_0}{g_i} \exp\left(\frac{E_i}{kT_{ex}}\right) \qquad (7)$$

with $g_0=5$.

Unfortunately, the energy level of absorbing state is 9.165 eV higher than the ground level. Therefore, estimated ground-level density might contain large errors.

5. Results

5.1 Test conditions

All tests were performed with pure oxygen plasma using 4 capacitors with a 2 μH coil (f = 0.74 MHz). The conditions were measured 393 mm downstream distance from the IPG exit.

Two different test cases were investigated:

Case 1a: The ambient pressure is 500 Pa, the oxygen mass flow rate 3 g/s, the anode voltage 6250 V and the anode power 106 kW. At this ambient pressure, the plume is not expanding and the plume diameter is almost the same as the heater exit at the measurement position. A photograph of IPG3 with this condition is shown in Fig. 1.

Case 1b: The measurement in front of the probe (Pitot pressure probe) under the conditions are the same as described for **case 1a**. Strong illumination region is limited to the very vicinity of the probe so that density profile could be obtained for the condition. Unfortunately, only information from the preliminary data processing is available for this condition (see below).

Case 2a: The ambient pressure is 50 Pa (i.e. facility base pressure), the oxygen mass flow rate 4 g/s, the anode voltage 6060 V and the anode power 83 kW. This condition is also known as the so-called FESTIP[1] condition.

Case 2b: Measurement using material sample holder system and Pitot probe measurement acc. to **case 2a**. Unfortunately, case 2 did not enable a feasible D-LAS measurement: Despite the strong absorption measured for cases 2a/b it was impossible to deduce the radial distribution because the information is limited near the axis i.e. the beam became to large such that a whole scan through the jet was not possible.

---

[1] Future European Space Transport Investigation Program; this plasma generator condition was used for SSiC material tests within the program.

5.2 Experimental results using the Pitot probe and the material support system

Table 2 below summarizes the conditions measured with the probes. For a approximation the Mach numbers were calculated one-dimensionally using the calculated ratio P_{pitot}/P_{amb}. Here, two cases must be considered. For the sub-sonic case the Mach number can be estimated using

$$1 + \frac{\kappa - 1}{2} M_{a1}^2 = \left(\frac{p_{tot}}{p_{amb}}\right)^{\frac{\kappa-1}{\kappa}} \qquad (8).$$

For the supersonic case we have to use

$$\frac{\frac{\kappa+1}{2} M_{a1}^2}{\left(\frac{2\kappa}{\kappa+1} M_{a1}^2 - \frac{\kappa-1}{\kappa+1}\right)^{\frac{1}{\kappa}}} = \left(\frac{p_{tot}}{p_{amb}}\right)^{\frac{\kappa-1}{\kappa}}, \qquad (9)$$

where κ is the adiabatic coefficient and M_{a1} is the Mach number. Both equations assume constant heat capacities. The static pressure is assumed to be the ambient pressure in the vacuum chamber. Hence, the measured pressure ratio leads to the Mach number in the form

$$Ma = f\left(\frac{P_{Pitot}}{P_{amb}}, \kappa\right). \qquad (10)$$

In Fig. 9 the resulting Mach numbers are illustrated. The full symbols show the interval calculated using equ. 8, while the empty symbols were calculated with equ. 9.
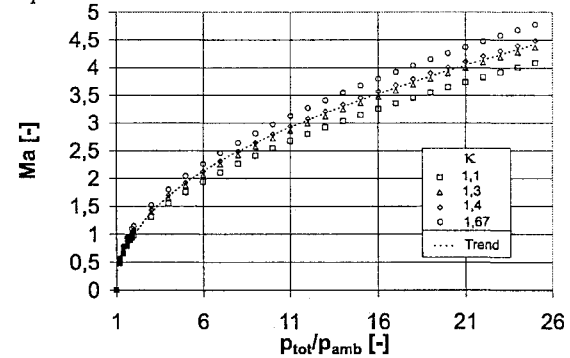
Fig. 9: Ma depending on pressure ratio p_{tot}/p_{amb}
The resulting values for the investigated test conditions are presented in table 2 below.

Table 2: Measured P_{Pitot}, T_{wall}, estimated Machnumbers

Case	P_A [kW]	P_{pitot} [Pa]	P_{pitot}/P_{amb}	T_{Wall} [°C]	Mach
1a	106	950	1.9	-	1.05
1b	106	950	1.9	1210	1.05
2a	83	190	3.8	-	1.6
2b	83	190	3.8	1050	1.6

For case 1b a material test using SSiC was performed (see Fig 10). This enables an estimative determination of the heat flux under this condition which is about

American Institute of Aeronautics and Astronautics

230 kW/m². During the test the ambient pressure was increased as shown in Fig. 10. The pressure control system swang over the 500 Pa threshold (above 600 Pa, thin black curve) which can be seen as temperature effect on the material sample as well. In fact, the temperature increases up to 1250 °C and decreases with the reach of the 500 Pa ambient pressure at t>=750 s (thick grey line).
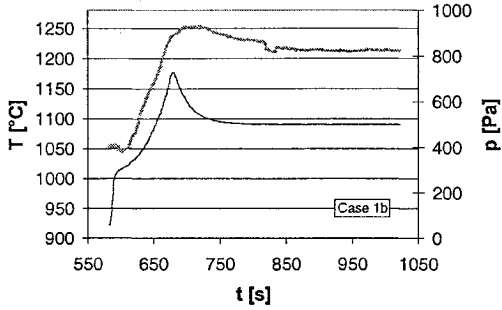
Fig. 10: Sample temperature and ambient pressure histories during the material test, x=393mm, p_{Pitot}=950 Pa (case 1b)

In Fig. 11 the anode voltage U_A can be seen in the same time interval. However, it is visible that the voltage has already been constant at t=650 s which implies that the temperature increase described above (see Fig. 10) is a pressure effect.
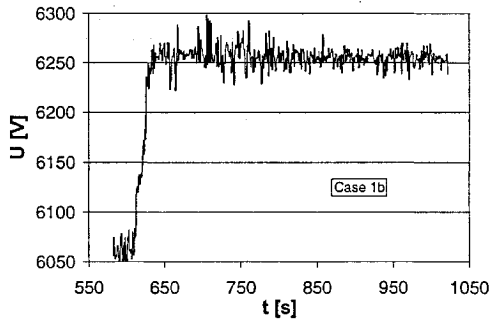
Fig. 11: anode voltage history during the material test, x=393mm, p_{Pitot}=950 Pa (case 1b)

Figure 12 depicts the Pitot pressure profile for case 2. The small, filled symbols mark the Pitot pressure while the large, empty symbols show the pressure ratio. The right side data points at about 400 mm show the measured Pitot pressures (this investigation). Additionally, the left side curves are shown from a former investigation. It can be seen that the whole condition is a super-sonic condition at rather high Machnumbers (compare Fig. 9).

Figure 13 shows the time history of the SSiC sample wall temperature for case 2b. Both the Pitot pressure and the temperature are in good agreement with the FESTIP condition measured at x=130 mm where a temperature of 1360 °C and a Pitot pressure of 340 Pa were reached (not reported in this paper).
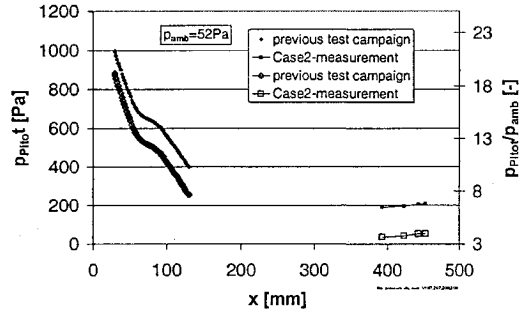
Fig. 12 Pitot pressure profile for case 2, the considered condition is at x=393 mm
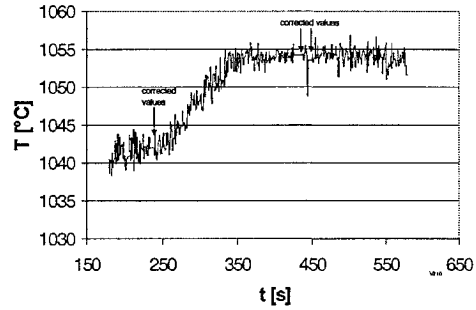
Fig. 13: Sample temperature history during the material test, x=393mm, p_{Pitot}=180 Pa (case 2b)

5.3 Experimental results using D-LAS

Scan data Case 1a

The oscillation frequency of the probe laser is scanned in two manners. The first one is the single-scan from 777 to 777.66 nm including the triplet absorption lines of atomic oxygen OI at 777.19, 777.41, 777.54 nm as shown in Fig. 14. The second one is the repetitive-scan using a function generator signal as shown in Fig. 15. The scan range is from 777.00 to 777.30 i.e. a range where the 777.19 nm line is.
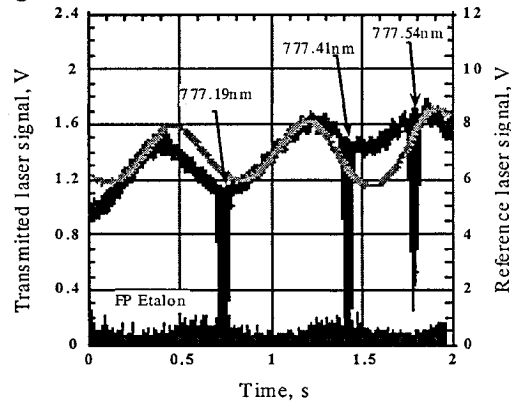
Fig. 14 Single-scan data.
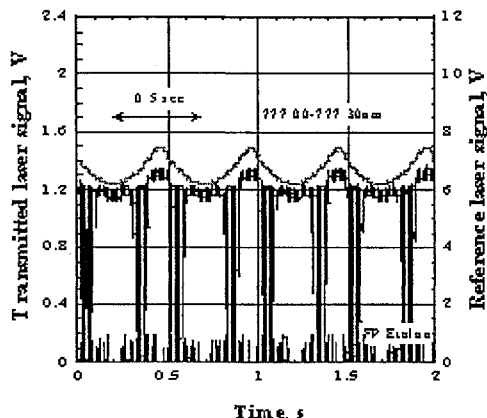
Fig. 15 Repetitive-scan data

Since the discharge current of the power source of PWK3 is regulated at the frequency of the 300 Hz [22], the data acquisition frequency must be higher than 300 Hz. However, the frequency sweep speed is not be high enough due to the limitation of mechanical control speed of a grating in a laser external cavity. Therefore, scan speed is set at low speed enough to catch each absorption peak. Then, time averaged profiles are obtained. The enlarged absorption profile near 777.19 nm is shown in Fig. 16. In the figure, alternate absorption at 300 Hz can be clearly seen.
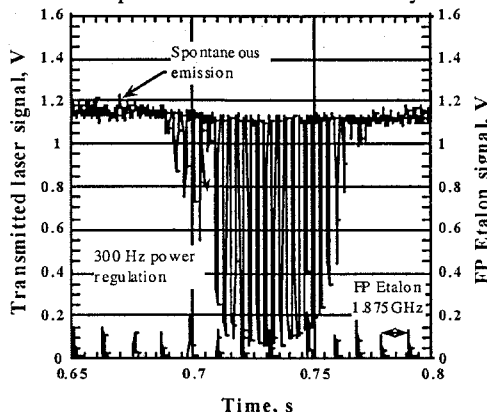
Fig. 16 An absorption signal at r=0 mm

The peaks must be interpolated to have plume properties during the operation. In the absorption profile, some peaks are missing. These miss-firings should be interpolated in data processing. The peaks of the etalon signal are spaced at an exactly 1.875 GHz interval. It is used for data conversion for time-base one to frequency–base one. There is some noise signal due to the spontaneous emission form the plume.

As seen in the figure, absorption fraction is approaching almost 100 %, and the plume is optically thick. In this region of absorption strength, the sensitivity would go down. (In order to avoid this insensitivity, we have an alternative to use the relatively week absorption line profile at 777.54 nm.)

Figure 17 shows the absorption signal 20 mm off axis. Many of the peaks are missing. This is due to the plume fluctuation at the frequency lower than 300 Hz. The plume diameter changes time by time, and this effect appears strongly at the edge of the plume.
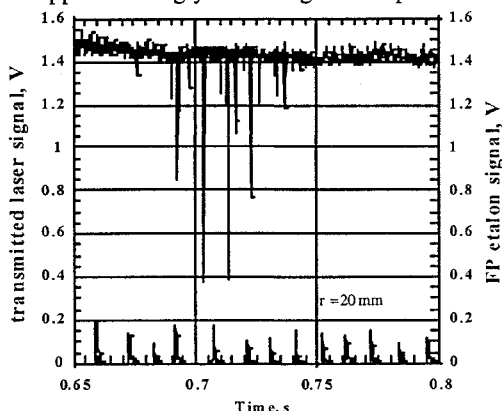
Fig. 17 An absorption signal at r=20 mm

By a curve-fit for this absorption profile, we will have time-averaged absorption intensity.

In this paper, only the single-scan data were used. Averaging the repetitive-scan data must give us more precise absorption profile.

Typical absorption profile Case 1a

The minimum values are selected out of the whole data, and then converted to frequency-based profiles using both the etalon signal and the reference beam-intensity variation. Figure 18 shows the absorption profiles at various radial positions. It showed very good frequency reproducibility.
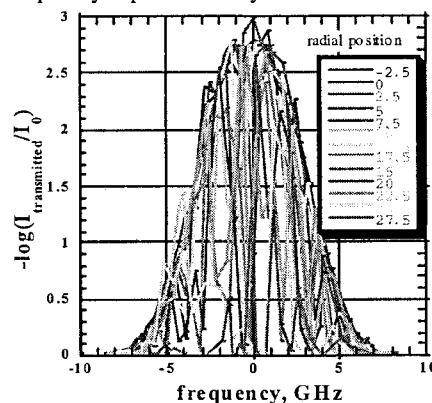
Fig. 18 Frequency-based absorption profile.

Then the minimum values are interpolated by fitting them to a 10th order polynomial as shown in Fig. 19
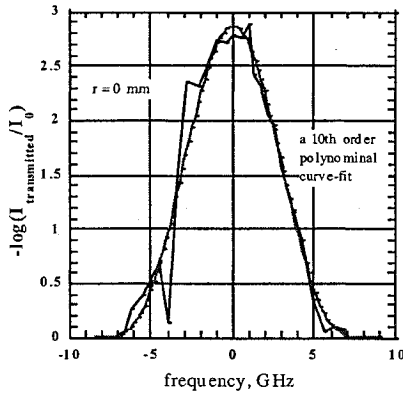
Fig. 19 Typical absorption profile.

Abel inversion Case 1a

To get the local absorption coefficient through Abel inversion, a derivative of absorption $d(-\ln(1-i(r)))/dr$ is required. The $-\ln(1-i(r))$ distribution is shown in Fig. 20. To avoid any positive gradient, the distributions are smoothed by 5th order polynomials.
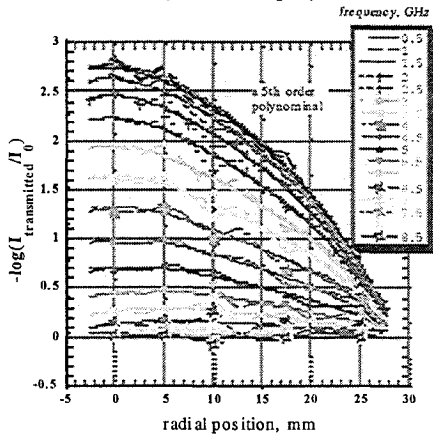
Fig. 20 Radial profile of absorption fraction.

Figure 21 shows the inverted absorption coefficient profiles. They should be fit to a Gaussian curve because the Doppler broadening is expected the predominant broadening mechanism so far.
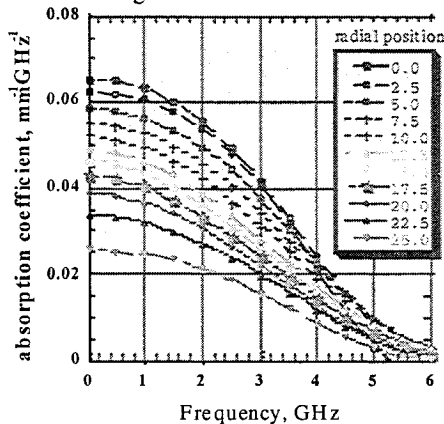
Fig. 21 Absorption coefficient profiles

Local properties Cases 1a and 1b

The local line width and total absorption coefficient (absorption coefficient integrated through the frequency) are available from the Gaussian curve fitting. The curve fittings at r =0 mm and 12.5 mm are shown in Fig. 22. At r =0 mm, fitting error is larger than the one at r =12.5 mm. This is thought partially because the measurement sensitivity is low near the axis due to the large optical thickness.
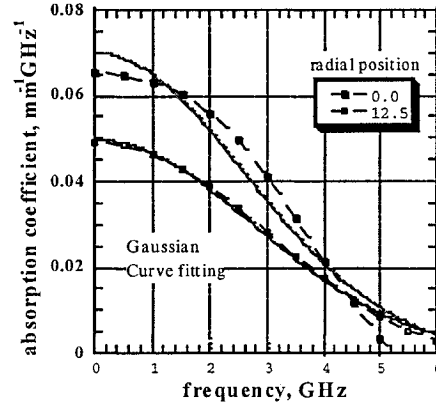
Fig. 22 Gaussian curve fitting.

Figure 23 shows the deduced distribution of number density of the atomic oxygen at the metastable level, at which the energy level is 9.165 eV higher than at the ground level.
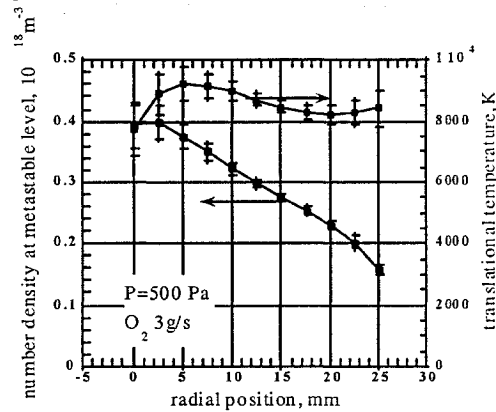
Fig. 23 Density and temperature distributions

The error bar indicates only the fitting error to the Gaussian curves. The maximum density is as much as $4 \cdot 10^{17}$ m^{-3} and the plume diameter defined by 1/e of maximum is 25 mm. The density is gradually decreasing with the radius. This would be due to the ambient-gas entrainment and also due to the fluctuation in plume diameter. These two effects cannot be separated in this time average measurement.

The translational temperature deduced from the Doppler broadening is shown in Fig. 23. It is estimated at 8000-9000 K. This would be enough high for full dissociation of oxygen gas

9

Estimation of ground level number density Cases 1a and 1b

Case 1a: The ground level number density of the atomic oxygen is estimated assuming the local thermal equilibrium. The Boltzmann plot is shown in Fig. 24.
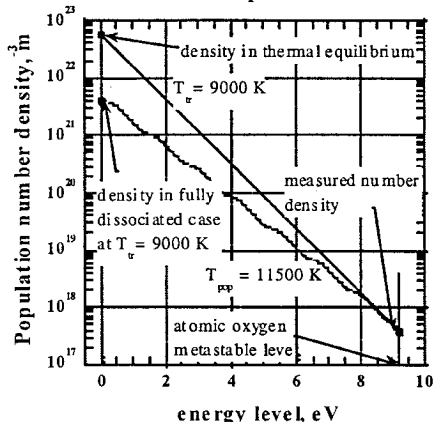
Fig. 24 Bolzmann plot

The predicted number density is $5.4 \cdot 10^{22}$, which is one order higher than the one calculated assuming full dissociation of oxygen. This indicates that the atomic oxygen is electronically under-populated Although precise degree of dissociation can not be determined from the plot, it is reasonable to think that the oxygen is fully dissociated by taking account of high translational temperature.

The population temperature defined by number densities at the ground level and the meta-stable level is 11500 K. This temperature would be preserved through the plume expansion and acceleration. The equilibrium temperature inside the inductive heater might be around 11500 K or higher.

Case 1b: Within a consideration of the raw data it was found that the number density of the absorbing level is almost same as that of Case 1a. This indicates that the shock is very weak or supports that the flow Mach number is about 1. A temperature profile in front of the probe can not be obtained because the flow is forced to go around the probe and Doppler shift due to this flow makes the broadening wider (flow components tangential to the probe surface.)

6. Summary

It has to be emphasized that we can not tell the exact number density of the ground level since the electronic excitation is found in nonequilibrium or under-populating (as shown in the Boltzmann plot). Accordingly, the consideration of the measured temperature is more important than number density.

Two test conditions with pure Oxygen plasmas were investigated in the inductively heated facility PWK3 using the plasma generator IPG3. For Case 1a at an ambient pressure of 500 Pa, an oxygen mass flow rate 3 g/s, an anode voltage 6250 V and an anode power 106 kW it could be determined that the jet is less expanding than in the low presssure case. By the inspection of the radial profiles at a distance of 393 mm from the IPG3 outlet a plasma jet diameter of 50 mm could be derived. The maximum density is as much as $4 \cdot 10^{17}$ m^{-3} and the radial temperatures are higher than 8000 K, which is high enough for the full dissociation of the Oxygen. Case 1b i.e. the measurement in front of the Pitot pressure probe under the conditions are the same as described for case 1a showed that the strong illumination region is limited to the very vicinity of the probe so that density profile could be obtained for the condition. However, only information from the preliminary data processing is presently available for this condition. A first analysis of the raw data showed that the number densities of the metastable level are almost the same as in case 1a. The Pitot pressure measured with the probe was 950 Pa. From the one-dimensional calculation using the tank pressure as ambient pressure a Mach number slightly above 1 can be derived. The similarity of the densities for both cases 1a and 1b confirms that the shock is very week or supports that the flow Mach number is about 1. Correspondingly, a SSiC material test was performed at the same condition. Here, SSiC temperatures of 1210 °C were measured leading to a partial catalytic heat flux of about 230 kW/m^2. The overal simulation point "case 1" can therefore be considered as quite well known. In order to discuss about the relationship between freestream temperature/enthalpy and heat flux to the probe, CFD assuming the surface catalysis has to be used in future. In case 2a ambient pressure is 50 Pa, oxygen mass flow rate is 4 g/s, anode voltage 6060 V and anode power 83 kW. The condition is also known as the so-called FESTIP condition. However, the FESTIP condition is at a position of 130 mm from the generator's outlet. Unfortunately, this position could not be measured due to interface reasons such that the position 393 mm was investigated under the same conditions. In this case strong absorption was measured as well but it was impossible to deduce the radial distribution as the beam's diameter was too large.

Pitot pressure and wall temperature on SSiC were measured as well (case 2b). Pitot pressure was about 180 Pa while temperature was at 1055 °C.

Acknowledgements

References

1. M. Auweter-Kurtz, H. L. Kurtz, S. Laure, "Plasma Generators for Re-entry Simulation", Journal of Propulsion and Power, Vol. 12, No. 6, Nov./Dez. 1996.

2. M. Auweter-Kurtz, M. Feigl, M. Winter: "Overview of IRS Plasma Wind Tunnel Facilities", Paper presented on the RTO AVT Course on "Measurement Techniques for High Enthalpy and Plasma Flows", Rhode-Saint-Genèse, Belgium, published in RTO EN-8, 25-29 October 1999.

3. G. Herdrich, M. Auweter-Kurtz, H. Kurtz, T. Laux, M. Winter: Operational Behavior of the Inductively Heated Plasma Source IPG3 for Re-entry Simulations, AIAA-99-3497, 33rd Thermophysics Conference, Norfolk, VA, June 1999.

4. Laux, T, Herdrich, G., Auweter-Kurtz, M.: "Material and Heat Flux Tests with Sintered Silicon Carbide in Oxygen and Nitrogen Plasmas", Proceedings of the „First Joint French-German Symposium on Simulation of Atmospheric Entries by Means of Ground Test Facilities, Paper 3.3, University of Stuttgart, Space Systems Institute, Nov. 1999.

5. T. Stöckle, M. Auweter-Kurtz, S. Laure, "Material Catalysis in High Enthalpy Air Flows", AIAA-96-1904, 31st AIAA Thermophysics Conference, New Orleans, LA, 1996.

6. G. Herdrich, M. Auweter-Kurtz, M. Hartling, T. Laux, "Present Design of the Pyrometric Sensor System PYREX-KAT38 for X-38", International Symposium on Atmospheric Reentry Vehicles and Systems, Arcachon, France, March 1999

7. M. Auweter-Kurtz, M. Feigl, M. Winter: "Diagnostic Tools for Plasma Wind Tunnels and Re-entry Vehicles at the IRS", Paper presented on the RTO AVT Course on "Measurement Techniques for High Enthalpy and Plasma Flows", Rhode-Saint-Genèse, Belgium, published in RTO EN-8, 25-29 October 1999.

8. F.-Y. Zhang, K. Komurasaki, T. Iida, T. Fujiwara: "Diagnostics of an Argon Arcjet Plume with a Diode Laser", Journal of Appplied Optics, Vol. 38, No. 9, pp. 1814-1822, 20 March 1999.

9. K. Komurasaki, M. Sugimine, S. Hosoda, Y. Arakawa: "Laser Absorption Measurement of Atomic Oxygen in Arc-Heater Plumes", Paper AIAA-2001-0814, Aerospace Sciences Meeting and Exhibit, 39th, Reno, NV, Jan. 8-11, 2001.

10. G. Herdrich, M. Auweter-Kurtz, H. Kurtz, T. Laux, E. Schreiber: "Investigation of the Inductively Heated Plasmagenerator IPG3 using Injection Rings of Different Geometries", AIAA-2000-2445, 21st Advanced Measurement Technology and Ground Testing Conference, Denver, CO, June 2000.

11. L. Maraffa, A. Smith, A. Santovincenzo, R. Rouméas, J.-P. Huot, G. Scoon, "Aerothermo-dynamics Aspects of Venus Sample Return Mission", 3rd European Symposium on Aerothermodynamics for Space Vehicles, ESTEC, Noordwijk, The Netherlands, ESA-SP 426, 24th-26th November 1998.

12. V. Rubio Garcia, L. Maraffa, G. Scoon, R. Rouméas, R. Seiler, "Mars Mini-Probes. Elements of Aerothermodynamics and Entry Trajectories", 3rd European Symposium on Aerothermodynamics for Space Vehicles, ESTEC, Noordwijk, The Netherlands, ESA-SP 426, 24th-26th November 1998.

13. W. O'Neil, Ch. Cazeau, "The Mars Sample Return Mission", IAF-99-Q.3.02, 50th International Astronautical Congress, Amsterdam, The Netherlands, Oct 1999.

14. F. Vilbig, "Lehrbuch der Hochfrequenztechnik", Vol. 2, Akademische Verlagsges. m. b. H., Frankfurt am Main 1958.

15. Technical Specification of the rf-capacitors and the Triode RS 3300 CJ of the PWK3-IPG energy supply, Fritz Düsseldorf Ges. m. b. H., 1997.

16. G. Herdrich, M. Auweter-Kurtz, H. Kurtz, "New Inductively Heated Plasma Source for Reentry Simulations", AIAA-98-3022, Paper presented on the 20th AIAA Advance Measurement and Ground Testing Conference, Albuquerque, NM, Juni 1998 and published in the Journal of Thermophysics and Heat Transfer, Vol. 14, No. 2, p. 244-249, April-June 2000.

17. Ch. Waters, "Current Transformers provide accurate, isolated Measurements", Pearson Electronics Report.

18. Mellon, M. G.: Analytical absorption spectroscopy (absorptimetry and colorimetry), John Willey & Sons, Inc., New York, pp. 78-98.

19. Zel'dovich, Y. B., Raizer, Y. P., Hayes, W. D. And Probstain, R. F.: Physics of shock waves and high-temperature hydrodynamic phenomena, Academic Press New York (1966), pp. 107-172.

20. Lochte-Holtgreven W.: Plasma Diagnostics, Norty-Holland Publishing Company, Amsterdam (1968), pp. 9-65.

21. Bear, D. S., Chang, H. A. and Hanson, R. K.: Semiconductor laser absorption diagnostics of atomic oxygen for atmospheric-pressure plasmas, AIAA paper 98-0822, 1998.

22. Fritz Düsseldorf GmbH, personal communication, 1998.